Scaling Behavior of Electronic Excitations in Assemblies of Molecules with Degenerate Ground States

H.-J. Fan,† C. Perkins,‡ and P. J. Ortoleva*,‡

Department of Chemistry, Prairie View A & M University, Prairie View, Texas 77446, and Department of Chemistry, Indiana University, Bloomington, Indiana 47405

Received: September 1, 2009; Revised Manuscript Received: November 20, 2009

The behavior of long space–time excitations in many-electron systems with ground state degeneracy is explored via multiscale analysis. The analysis starts with an ansatz for the wave function's dual dependence on the N-electron configuration (i.e., both by direct means and by indirect means via a set of order parameters). It is shown that a Dirac-like equation form of the wave equation emerges in the limit where the ratio ε (of the average nearest-neighbor distance to the characteristic length of the long-scale phenomenon of interest) is small. Examples of the long scale are the size of a quantum dot, nanotube, or wavelength of a density disturbance. The velocities in the Dirac-like equation are the transition moments of the single-particle momentum operator connecting degenerate ground states. While detailed band structure and the independent quasi-particle picture could underlie the behavior of some systems (as commonly suggested for graphene), the present scaling law results show it is not necessarily the only explanation. Rather, it can follow from the scaling properties of low-lying, long spatial scale excitations and ground state degeneracy, even in strongly interacting systems. The generality of our findings suggests graphene may be just one of many examples of Dirac-like equation behavior. A preliminary validation of our quantum scaling law for molecular arrays is presented. As our scaling law constitutes a coarse-grained wave equation, path integral or other methods derived from it hold great promise for calibration-free, long-time simulation of many-particle quantum systems.

I. Introduction

A noninteracting quasi-particle picture has been used to suggest that electrons in graphene satisfy an equation similar in character to that of Dirac for relativistic fermions.[1] This has been justified on the basis of a detailed analysis of band structure and Fermi surface topology. However, since electrons at high density interact strongly, some doubt remains as to the nature of graphene and the possible more widespread occurrence of Dirac-like behavior, including the proportionality between excitation energy and wave vector.

The notion that strongly interacting quantum systems can be understood via a multiscale analysis of the Schrödinger equation has been explored for boson and fermion systems.[2,3] The implication of this deductive approach is that a coarse-grained function emerges that satisfies a wave equation similar in form to the original Schrödinger equation, but with modified masses and interparticle forces. The question remains as to whether a Dirac-like equation (with first-order spatial derivatives and not second-order ones) could also emerge from scaling arguments. Here, Dirac-like equations are derived for many-fermion systems with arbitrary interaction strength. The theory starts with an ansatz for the wave function's dependence on the N-particle configuration, i.e., both by direct means and by indirect means via a set of order parameters. A multiscale approach based on this ansatz yields a coarse-grained wave equation with Dirac-like character under specified, but rather general, conditions.

Coarse-grained equations for N-particle Newtonian systems have been derived via multiscale analysis of the classical Liouville equation.[4−11] This approach starts with an ansatz on the dependence of the N-particle probability density. Here, we extend this theme to quantum systems, deriving a coarse-grained wave equation with modified Dirac character via multiscale analysis of the N-fermion wave equation.

The Dirac equation describes the dynamics of a set of wave functions. The question arises as to how a set of wave equations could arise from the single Schrödinger equation that is the starting point of our analysis. The possibility of such behavior already emerged in the classical N-atom problem when there were multiple conserved or other slow variables involved in the phenomenon of interest.[6] In the present development, we show that the analogue of this effect is the existence of ground state degeneracy, and its implications for the behavior of low-lying, long-scale excitations from them.

The overall objective of the present study is to derive a scaling law for many-fermion systems and demonstrate it for electron phenomena. We start with an ansatz on the behavior of the wave function and a scaling parameter, notably the ratio ε of the average nearest-neighbor distance to the characteristic length of the phenomenon of interest (e.g., the size of a nanoparticle or wavelength of a density disturbance). The ansatz on the wave function, and the appearance of ε in the wave equation that results from it, enables an analysis that results in a coarse-grained wave-equation for long-scale excitations from the ground state. This course-grained equation enables one to validate the original ansatz via a self-consistency argument. It also implies a numerical scheme to simulate the long-time dynamics of many-fermion systems over long time periods.

Path integral methods have been used to simulate quantum systems.[12] However, the time steps required (e.g., 10^{-14} s) severely limit the applicability of the method when many-particle, long-time processes, and calibration-free theory are of interest. In contrast, a path integral approach based on a coarse-

* Corresponding author. E-mail: ortoleva@indiana.edu.
† Prairie View A & M University.
‡ Indiana University.

10.1021/jp908441s
Published on Web 01/19/2010

grained wave equation only requires a long time step, i.e., one related to the long-time phenomenon of interest.

In our approach to many-particle quantum or classical systems, we identify order parameters, i.e., variables that track the larger scale motions of particles singly or collectively. We make the ansatz for the dependence of the wave function on the N-particle configuration both by direct means and by indirect means via the order parameters. The ansatz is then tested by (1) demonstrating that the wave equation does yield such solutions and (2) determining conditions under which this ansatz is self-consistent. We demonstrate self-consistency when (1) the ratio of the average nearest-neighbor distance to the length-scale characteristic of the phenomenon of interest (e.g., the size of a nanotube or nanowire) is small and (2) the system is close to the ground state.

Derivation of the scaling law for Dirac-like behavior is presented (section II). Properties and general implications of the law are provided (section III). A preliminary validation of the scaling law is attained via standard quantum computations (section IV). Conclusions are drawn (section V).

II. Deriving the Dirac-Like Scaling Law via Deductive Multiscale Analysis

In analogy with other multiscale approaches to quantum[2,3] and Newtonian[4−11] many-particle systems, we start with an ansatz on the wave function Ψ and derive a coarse-grained wave equation. The result is that many-particle systems display one of a set of long space−time behavior depending on the nature of the particles and their interactions. Here we focus on one such scaling law that, despite the second-spatial derivative nature of the Schrödinger equation, is first-order in spatial gradients.

Consider an N-fermion system described by the configuration $\underline{r} = \{\vec{r}_1, ..., \vec{r}_N\}$. However, Ψ can have multiple types of dependencies on $\underline{r}$, e.g., that describing variations on the scale of the average nearest-neighbor distance, and that from the size of a large cluster, a droplet, or the wavelength of a density disturbance. Let ε be the ratio of the average nearest-neighbor distance to the characteristic length of the aforementioned phenomena. For example, consider a one-dimensional array of molecules of length L, while l is the size of one molecule in the array. In that case, $\varepsilon = l/L$. An objective of the present analysis is to determine how low-lying excitations from the ground state of the overall system behave for smallε. We make the ansatz that Ψ depends on both $\underline{r}$ and $\underline{R} \equiv \varepsilon\underline{r}$, the latter characterizing large-scale phenomena. This is not a violation of the number of degrees of freedom; rather, it is an expression of the multiple distinct ways in which Ψ depends on $\underline{r}$. In like manner, we expect Ψ can depend on time t both directly and, through a set of scaled times $\underline{t} = \{t_1, t_2, ...\}$ for $t_n = \varepsilon^n t$, indirectly. Letting $t_0 = t$ to symmetrize the notation, we arrive at the multiscale ansatz

$$\Psi(\underline{r},\underline{R},t_0,\underline{t};\varepsilon) \tag{1}$$

Our objective is to show that this dependence can be self-consistently constructed for small ε. This is the starting point of our derivation of a scaling law for many-fermion systems.

The wave equation for N-identical fermions is

$$i\hbar\frac{\partial\Psi}{\partial t} = H\Psi \tag{2}$$

$$H = K + V \tag{3}$$

for kinetic and potential energy operators K and V. When the ansatz (1) is placed into the wave equation (2), the chain rule implies

$$i\hbar\sum_{n=0}^{\infty}\varepsilon^n\frac{\partial\Psi}{\partial t_n} = (H_0 + \varepsilon H_1 + \varepsilon^2 H_2)\Psi \tag{4}$$

The form of the operators H_0, H_1, and H_2 follow from (1) and the chain rule. Let the potential V be written $V_0 + \varepsilon V_1 + \varepsilon^2 V_2$ as discussed further below. With this, the Hamiltonian operators take the form

$$H_0 = -\frac{\hbar^2}{2m}\underline{\nabla}_0{}^2 + V_0(\underline{r},\underline{R}) \qquad H_1 = -\frac{\hbar^2}{m}\underline{\nabla}_0\cdot\underline{\nabla}_1 + V_1$$
$$H_2 = -\frac{\hbar^2}{2m}\underline{\nabla}_1{}^2 + V_2(\underline{r},\underline{R}) \tag{5}$$

where $\underline{\nabla}_0$ and $\underline{\nabla}_1$ are gradients with respect to $\underline{r}$ at constant $\underline{R}$ and with respect to $\underline{R}$ at constant $\underline{r}$, respectively; $\nabla_0{}^2$ and $\nabla_1{}^2$ are the corresponding Laplacians. The operator H_0 is a Hamiltonian describing the short space−time dynamics of the system and follows from the choice of V_0, the N-particle potential with long-scale interactions removed. H_1 and H_2 emerge from the ansatz (1), the chain rule and that $V = V_0 + V_1\varepsilon + V_2\varepsilon^2$, where $V - V_0$ accounts for the long-scale interactions (see below).

In what follows, we solve (4) as an expansion in ε, i.e., $\Psi = \sum_{n=0}^{\infty}\varepsilon^n\Psi_n$. It is the explicit appearance of ε in the reformulated wave eq 4 that enables the multiscale analysis.

Our focus is on slowly varying disturbances from the ground state, i.e., taking the convention that the ground state energy is zero, Ψ is independent of t_0 as $\varepsilon \to 0$. In this case, the lowest order wave function in the small ε analysis, Ψ_0, takes the form

$$\Psi_0 = \hat{\Psi}_{\hat{k}}(\underline{r},\underline{R})\, W_k(\underline{R},\underline{t}) \tag{6}$$

where $\hat{\Psi}_k$ is the kth of the N_d degenerate ground states of H_0 ($k = 1, ..., N_d$). The ground state, and hence V_0, is chosen such that $H_0\hat{\Psi}_k = 0$ for $k = 1, ..., N_d$. The factors $W_k(\underline{R},\underline{t})$ will be shown to be coarse-grained wave functions and are determined as follows.

To $O(\varepsilon)$ the multiscale wave equation implies

$$\left(i\hbar\frac{\partial}{\partial t_0} - H_0\right)\Psi_1 = -i\hbar\frac{\partial\Psi_0}{\partial t_1} + H_1\Psi_0 \tag{7}$$

This equation admits the solution

$$\Psi_1 = S(t_0)\Psi_1^o - i\hbar t_0 \sum_{k=1}^{N_d} \hat{\Psi}_k \frac{\partial W_k}{\partial t_1} - \sum_{k=1}^{N} \int_{-t_0}^{0} dt_0' S(-t_0') H_1(\hat{\Psi}_k W_k) \quad (8)$$

Here $S(t_0)$ denotes the evolution operator $\exp(-iH_0t_0/\hbar)$; Ψ_1^o is the initial value of Ψ_1 (i.e., at $t_0 = 0$). Constraints on the value of Ψ_1^o are only relevant when the development of $O(\varepsilon^2)$ is considered; a more complete discussion of this point has been presented in the context of the classical Liouville equation.[10]

To further the analysis, we introduce the complete set of eigenstates $|k\rangle$ of H_0. By definition, $H_0|k\rangle = \zeta_k|k\rangle$ for energy ζ_k. For $k = 1, ..., N_d$, $\zeta_k = 0$ as these are taken to be the N_d degenerate ground state wave functions (denoted alternatively $\{\hat{\Psi}_1, ..., \hat{\Psi}_{N_d}\}$). One may express $\Omega|k\rangle$ for arbitrary operator Ω in the $|k\rangle$:

$$\Omega|k\rangle = \sum_{k'=1}^{\infty} |k'\rangle\langle k'|\Omega|k\rangle \quad (9)$$

Completeness of the set of $|k\rangle$, and the fact that the long-time average of $S(-t_0)|k\rangle$ for $\zeta_k \neq 0$ vanishes, imply

$$\lim_{t_0\to\infty} \frac{1}{t_0} \int_{-t_0}^{0} dt_0' S(-t_0')\Omega|k\rangle = \sum_{k'=1}^{N_d} |k'\rangle\langle k'|\Omega|k\rangle \quad (10)$$

This long-time-expectation equivalence theorem plays a role in the present multiscale analysis of quantum systems similar to that of the Gibbs hypothesis for statistical mechanics as applied to the analysis of the classical Liouville equation.[9] Examination of (8) shows t_0-divergent terms that signal the breakdown of the development unless such terms counterbalance each other. Thus if Ψ_1 is well-behaved as $t_0 \to \infty$, then the following condition must be met:

$$i\hbar \sum_{k=1}^{N_d} |k\rangle \frac{\partial W_k}{\partial t_1} = -\frac{1}{m} \sum_{k,k'=1}^{N_d} \sum_{l=1}^{N} |k\rangle\langle k|\vec{p}_l\rangle \cdot \vec{p}_l(W_k|k'\rangle) + \sum_{k'=1}^{N_d} \langle k|V_1|k'\rangle W_{k'} \quad (11)$$

Since each $|k\rangle$ component ($k = 1, ..., N_d$) of the equation must hold, boundedness of Ψ_1 implies

$$i\hbar \frac{\partial W_k}{\partial t_1} = \frac{\hbar}{m} \sum_{k'=1}^{N_d} \sum_{l=1}^{N} \langle k|\vec{p}_l\rangle \cdot \frac{\partial (W_{k'}|k'\rangle)}{\partial \vec{R}_l} + \sum_{k'=1}^{N_d} \langle k|V_1|k'\rangle W_{k'} - \frac{1}{m} \sum_{k'=1}^{N_d} \sum_{l=1}^{N} \langle k|\vec{p}_l \cdot \frac{\partial}{\partial \vec{R}_l}|k'\rangle W_{k'} \quad (12)$$

Exchange antisymmetry of the fermion system implies the W_k are boson-like functions since the $|k\rangle$ are antisymmetric. We suggest that (12) constitutes a Dirac-like model when the $\underline{R}$-dependence of the factors involving the momentum terms is weak, and is a more complex analogue for the general case.

An example of how V can be expressed in the form $V_0 + \varepsilon V_1$ is as follows. Consider the Coulomb $1/r$ potential. Rewrite it via $1/r = e^{-\varepsilon\kappa r}/r + (1 - e^{-\varepsilon\kappa r})/r$, for κ on the order of the average nearest neighbor distance. Let $R = \varepsilon r$ so that the Coulomb interaction is now $e^{-\kappa R}/r + \varepsilon(e^{-\kappa R} - 1)/R$. More generally, the exponential factor can be replaced by a decaying function $f(\varepsilon r)$. With this formulation and an external potential from ion cores on a lattice, electronic excitations can be addressed with the present multiscale scheme.

III. Properties of the Generalized Dirac-Like Scaling Law

A. Role of Antisymmetry. Antisymmetry of the ground states $|k\rangle$ places strong constraints on the behaviors implied by the scaling law of section II. A qualitative difference in the implications of antisymmetry arises from cases with $|k\rangle$ independent of, versus dependent on, $\underline{R}$.

Case I: $|k\rangle$ Independent of $\underline{R}$. Define $F_{lkk'}$ via

$$F_{lkk'} = \langle k|\vec{p}_l \cdot \vec{P}_l(W_{k'}|k'\rangle) \quad (13)$$

If $|k\rangle$ is independent of $\underline{R}$, antisymmetry and relabeling dummy integration variables imply

$$F_{lkk'} = \frac{\hbar \vec{u}_{kk'}}{i} \cdot \frac{\partial W_{k'}}{\partial \vec{R}_l} \qquad \vec{u}_{kk'} = \langle k|\vec{p}_l|k'\rangle \quad (14)$$

and the velocity-like variable is independent of l. This can be seen more explicitly when writing out the matrix element $\langle k|\vec{p}_l|k'\rangle$ in terms of the spatial representation $\hat{\Psi}_k$ of the ground state wave functions (see below). Since $\vec{u}_{kk'}$ is l-independent for the present case, the $F_{lkk'}$ term in the scaling law corresponds to a pervasive flow. Thus, there is a velocity $\vec{u}_{kk'}$ whose direction is related to the ground states.

Case II: $|k\rangle$ Dependent on $\underline{R}$. For this situation

$$F_{lkk'} = \langle k|\vec{p}_l|k'\rangle \cdot \vec{P}_l W_k + W_{k'}\langle k|\vec{p}_l \cdot \vec{P}_l|k'\rangle \quad (15)$$

The l-dependence of the second term is as follows.

$$\gamma_{kk'} = -\hbar^2 \int d^{3N}r\, \hat{\Psi}_k^*(\vec{r}_1,\vec{R}_1,...,\vec{r}_N,\vec{R}_N) \frac{\partial}{\partial \vec{r}_l} \cdot \frac{\partial}{\partial \vec{R}_l} \hat{\Psi}_{k'}(\vec{r}_1,\vec{R}_1,...,\vec{r}_N,\vec{R}_N) \quad (16)$$

For $l = 1$, for example, an auxiliary quantity $a_{lkk'}$ is introduced as follows

$$\frac{\hbar}{i} a_{1kk'} = \langle k|\vec{p}_1|k'\rangle = \frac{\hbar}{i} \int d^{3N}r\, \hat{\Psi}_k^*(\vec{r}_1,\vec{R}_1,...,\vec{r}_N,\vec{R}_N) \frac{\partial}{\partial \vec{r}_l} \hat{\Psi}_{k'}(\vec{r}_1,\vec{R}_1,...,\vec{r}_N,\vec{R}_N) \quad (17)$$

By antisymmetry

$$a_{1kk'} = \int d^{3N}r\, \hat{\Psi}_k^*(\vec{r}_1,\vec{R}_2,\vec{r}_2,\vec{R}_1,...,\vec{r}_N,\vec{R}_N)\frac{\partial}{\partial \vec{r}_2} \cdot \frac{\partial}{\partial \vec{R}_1}\hat{\Psi}_k(\vec{r}_1,\vec{R}_2,\vec{r}_2,\vec{R}_1,...,\vec{r}_N,\vec{R}_N) \quad (18)$$

While $\vec{r}_1$ can be renamed $\vec{r}_2$, and conversely for $\vec{r}_2$ since $\underline{r}$ is being integrated over, it is seen that $\vec{R}_1$ and $\vec{R}_2$ cannot be relabeled in a similar manner since they are not integrated over. Thus $\gamma_{lkk'}$, and similarly $\langle k|\vec{p}_l|k'\rangle$, depend on l

$$F_{lkk'} = \vec{u}_{kk'}\frac{\partial W_{k'}}{\partial \vec{R}_l} + \gamma_{kk'}W_{k'} \quad (19)$$

Both Cases. Antisymmetry places strong constraints on the implications of the scaling law. As $\vec{u}_{kk'}$ is independent of l and $\underline{R}$ when the $|k\rangle$ are independent of $\underline{R}$, all particles move coherently and lose all identity. When the $|k\rangle$ are $\underline{R}$-dependent, the dynamics is more complex. That $\gamma_{lkk'}$ is l-dependent implies the dynamics varies across the system (due to the $\underline{R}$ dependence of $\langle k|\vec{p}_l|k'\rangle$).

B. Role of Long-Scale Dependence. As shown in the above, the $\underline{R}$ dependence of the ground states preserves some measure of particle label identity in the $\langle k|\vec{p}_l|k'\rangle$. This $\underline{R}$-dependence can arise not only from the separation of the potential energy into long and short-scale contributions (as in section II) but also from the finite size of a system (e.g., a quantum dot, superconducting nanowire, cluster of molecules with degenerate ground states). To illustrate the latter, but not to restrict the applicability of the present formulation, $\hat{\Psi}_k$ can be in the form of a Slater determinant of single-particle functions Ψ. The latter could, for illustrative purposes, be written $\Psi^s(\vec{r},t)\,\Psi^l(\vec{R},t)$ where superscripts s and l indicate short and long scale dependence. The Ψ^l factor confines the particle to the finite system while Ψ^s provides the short-scale structure required to accommodate the exclusion principle. Dependence of $|k\rangle$ on $\vec{R}$ could also be created by the imposition of an external field.

C. Traveling Waves. Consider linear arrays of molecules with degenerate ground states. The long-scale behavior required as noted in subsections IIIA,B are provided here via the length of the array of molecules. We suggest that traveling wave concepts could apply since molecules are 3-D objects; the terminal molecules at the end of the linear array could provide a pivot point around which electrons can be redirected back along the array. Thus the linear array of 3-D objects can be described via periodic boundary conditions as applied to the electron motion. In a similar way, leading to a slightly more complex analysis than that presented below, excitations could propagate across a spherical quantum dot.

When $|k\rangle$ is independent of $\underline{R}$, there are factorized solutions to (12) if V_1 is zero, i.e.,

$$W_k = \prod_{l=1}^{N} w_k(\vec{R}_l,\underline{t}) \quad (20)$$

The single particle functions $w_k(\vec{R},\underline{t})$ satisfies

$$\frac{\partial w_k}{\partial t_1} + \sum_{k'=1}^{N_d}\vec{u}_{kk'} \cdot \frac{\partial w_{k'}}{\partial \vec{R}} = 0 \qquad m\vec{u}_{kk'} = \langle k|\vec{p}_l|k'\rangle \quad (21)$$

Traveling wave solutions for the case of $\underline{R}$-independent $|k\rangle$ can be obtained since $\vec{u}_{kk'kk'}$ is $\underline{R}$-independent:

$$w_k(\vec{R},t_1) = B_k \exp(i[\vec{q} \cdot \vec{R} - \omega t_1]) \quad (22)$$

These traveling waves exist when there are nontrivial solutions for the B_k:

$$\sum_{k'=1}^{N_d}[\omega\delta_{kk'} - \vec{q} \cdot \vec{u}_{kk'}]B_{k'} = 0 \quad (23)$$

This implies the dispersion relation

$$\det[\omega \mathbf{I} + \vec{q} \cdot \mathbf{u}] = 0 \quad (24)$$

For those solutions to exist, ω must be real for some range of $\vec{q}$ that is determined by the structure of $\vec{u}_{kk'}$.

IV. Validating and Interpreting the Scaling Law

A study of arrays of interacting molecules was undertaken using Gaussian 03[13] to assess the scaling law of section II and to derive its implications for excitations in many-electron systems. We focus on our conjecture that molecules with degenerate ground states (of which there are many[14−18]) can display Dirac-like behavior when assembled in an array. C_3H_3 was selected for this assembly study because it is small and has multiple ground states. The frontier orbital of C_3H_3 has E″ symmetry according to its D_{3h} point group (Figure 1). The main character of these two degenerate E″ orbitals is from the carbon's p-orbital. Both *E*″ orbitals are π-type, being either an in-phase or out-of-phase combination of these p-orbitals (bottom of Figure 1). With a single electron to fill these two degenerate E″ orbitals, the system supports two electronic configurations (ground states). One state has the single electron in the first of two degenerate E″ orbitals (state 1), while the electron is in the other for state 2 (Figure 1).

Quantum mechanical (QM) computations were carried out using DFT (density functional theory) via Gaussian 03 because it has the accuracy to reproduce results similar to ab initio methods but with less CPU time. The geometry-optimization on C_3H_3 was carried out with the Becke hybrid exchange functional and the Lee−Yang−Parr correlation function (B3LYP).[19,20] These calculations were performed with the Pople basis sets (6-31++G(d′,p′)[21−24] polarization functions (denoted "d", "p", for angular flexibility to represent regions of high electron density among bonded atoms).[25] The diffuse function, which represents the tail portion of the orbital, was added to both carbon and hydrogen to account for the long-distance interactions among the C_3H_3 that we expect to be relevant for long-scale excitations.

Electron density was examined to determine configurations favoring electron hopping between neighboring C_3H_3 units and across the assembly. Arrays of favorably oriented C_3H_3 units were simulated and excited states examined computationally. Linear arrays of up to 30 C_3H_3 were configured on the basis of

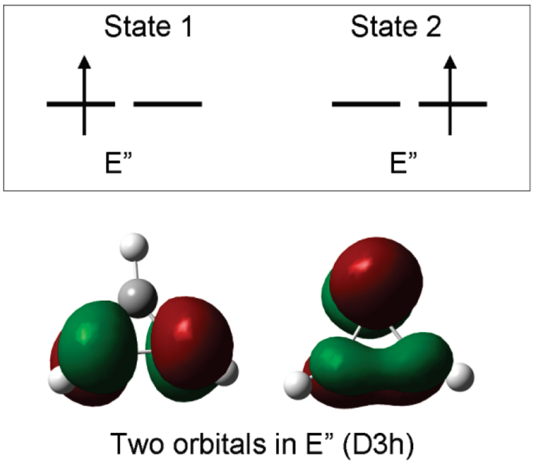

Figure 1. Schematic representation of two degenerate states (states 1 and 2) of C_3H_3 (above). The shape and nodal representation of these two E″ orbitals are also shown (below).

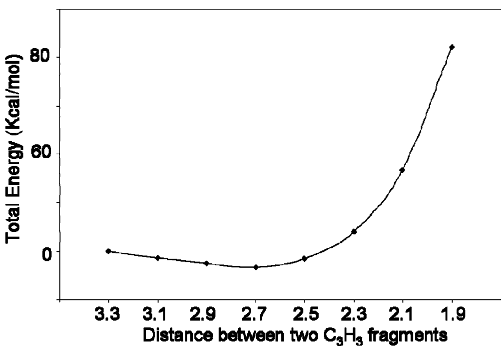

Figure 2. Total energy vs distance between two C_3H_3 molecules. The energy stabilizes slowly before 2.7 Å and rises up rapidly when the distance of two C_3H_3 molecules further decreases.

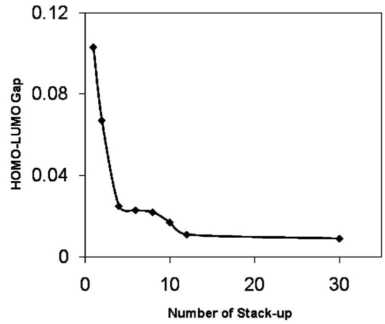

Figure 3. HOMO−LUMO gap versus the number of C_3H_3 molecules in a linear array calculated using Gaussian 03 with 6-31++G(d′,p′) and the B3LYP method.

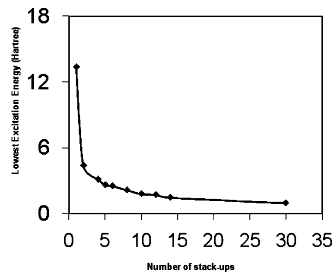

Figure 4. ZINDO simulation of the lowest excitation energy of C_3H_3 molecules in a linear array for up to 30 C_3H_3.

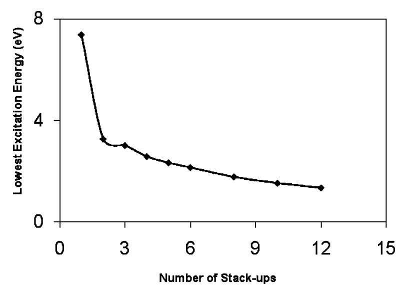

Figure 5. TD-DFT simulation of the lowest excitation energy of C_3H_3 molecules in a linear array was limited to 12 molecules due to computational cost. Calculations were carried out by Gaussian 03 using 6-31++G(d′,p′) with the B3LYP method.

optimized-geometry by the aforementioned QM methods. Spacing between C_3H_3 molecules was determined to be at 2.7 Å (Figure 2). The total energy of two C_3H_3 molecules slowly decreases as two molecules approach each other and then rises up rapidly after 2.5 Å.

These C_3H_3 molecules are arranged along the *c*-axis (Figure 6), all having the same orientation but translated in the *c*-direction to provide the linear array structure. There is no chemical bond formed at 2.7 Å, but there is a minimum in total energy, as shown in Figure 2. Excitation energy as a function of the number of C_3H_3 in a linear array provided a test of the scaling law of section II. We investigated three approaches for estimating the excitation energy: (a) the energy difference between the highest occupied molecular orbital (HOMO) and lowest unoccupied molecular orbital (LUMO), (b) the excitation energy from the semiempirical Hartree−Fock intermediate neglect of differential overlap method (ZINDO),[26] and (c) excitation energies of the lowest excited states from time-dependent DFT (TD-DFT).[27] Both the ZINDO and time dependent density functional theory (TD-DFT) methods have been widely used in studying the absorption wavelength of conjugated systems[28−30] these studies show that TD-DFT provides an efficient means for computing excited states of chemical systems.[31−33] Some studies show remarkable agreement with the experimental results such as UV−vis.[34−37]

Examining simple cases of the scaling law (11) suggests that the excitation energy should vary inversely with the number of molecules in a linear array (Figures 3−5 and section IIIB). Although the HOMO−LUMO gap follows the same trend as that predicted from ZINDO and TD-DFT (Figure 3), the values of the excitation energies do not agree quantitatively. A recent study shows that TD-DFT methods generally are more accurate than ZINDO in predicting the UV absorption spectra of delocalized molecules such as phenylamino compounds; predictions improve when diffuse functions were added to the basis functions.[28] The electronic transition properties simulated here include the maximum excitation energy (eV) and corresponding oscillator strengths. For comparison, only the first transition with minimum oscillator strength of 0.1 was considered. We encountered similar computational cost and convergence difficulties due to the size and symmetry imposed as reported in ref 38; therefore, TD-DFT results were only obtained for up to 12 C_3H_3 molecules.

While predicted excitation energy decreases with the increasing number of molecules in the linear array (as suggested by section section IIIB), eventually in our preliminary simulations the excitation energy fluctuates (Figures 3 and 5). This fluctuation is likely a consequence of numerical difficulties due to the low excitation energy and inaccuracies in the QM method used.

Next we used the QM optimized geometry to build a periodic array of C_3H_3 molecules. Two types of periodic cells (rectangle shape with symmetry of P1) were used: one cell has parameters

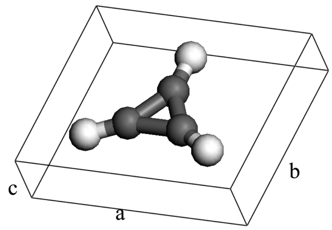

Figure 6. Schematic depiction of the cell (a, b, c) used in periodic array simulations.

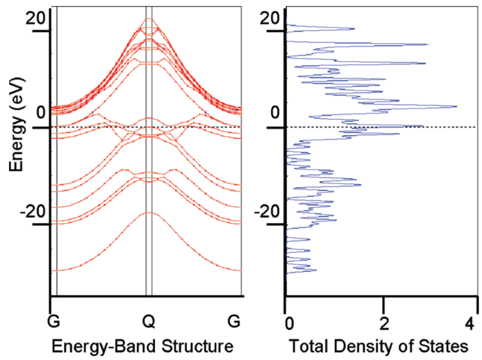

Figure 7. Electronic structure of the cell used to generate a 3-D array of C_3H_3 with $a = b = 20$ Å and $c = 1.35$ Å. The energy-band structure on the left is measured from the Fermi energy level (dotted line) and plotted along the c-direction of the cell in reciprocal space; the corresponding total DOS is plotted on the right.

of $a = b = 20$ Å and $c = 1.35$ Å (Figure 6). This corresponds to face-to-face C_3H_3 distance of 2.70 Å, the same as that for the above QM simulations. The values of a and b were adopted to ensure the cell was large enough (20 Å) to isolate the linear array of C_3H_3 molecules; the other type of periodic cell was for $a = 6$, $b = 5$ and $c = 1.35$ Å.

Differences in the electronic structure between these two cells provides additional information on the interaction among C_3H_3 units. Because this cell is repeated along the a, b, and c directions, the cell with $a = b = 20$ Å closely approximates linear arrays of C_3H_3 units too far apart to have any interaction along the a or b direction. DFT calculations were performed on these two types of cells to produce band structure and density of states (DOS). All calculations were performed using the CASTEP module in Accelry's Material Studio 4.1,[39] with which we used a gradient-corrected (GGA) functional for the plane-wave expansion of the single particle wave function and PW91 exchange-correlation potentials.[40] Polarized spin was used in the simulation because of the open-shell of C_3H_3. An energy cutoff of 310 eV was used for the plane wave basis set and the Brillouin zone was represented by 180 points in reciprocal space.

In Figure 7 we show the energy-band structure for the large cell ($a = b = 20$ Å) for the periodic array of C_3H_3 units, equivalent to a one-dimensional array of C_3H_3 units along the c-direction. The energy-band structure plot shows the strong interaction and delocalization of the valence electrons. The DOS plot on the right shows the nonzero density of states at the Fermi level, suggesting no energy gap. This agrees with the prediction that excitation energy should decrease with increasing number of units in the linear array. The band structure and DOS plot of the smaller cell ($a = 6$, $b = 5$ Å) reveals band features (not shown) similar to those of Figure 7 for the large cell ($a = b = 20$ Å). However, the intensity of the DOS of the smaller cell is 0.5 eV less than that of the large cell. This could contribute to possible interactions along the a- and b-directions in the small cell that remove electrons from the π-frontier orbitals.

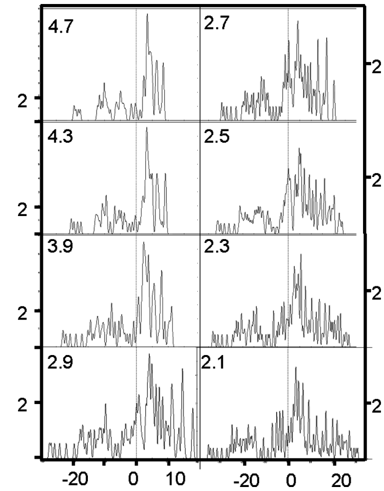

Figure 8. DOS of C_3H_3 units in a linear array with different cell sizes (fixed $a = 20$, $b = 20$, and c ranging from 2.1 to 4.7 Å). The horizontal-axis is the energy level and the vertical axis is the DOS. The dotted line indicates the Fermi level.

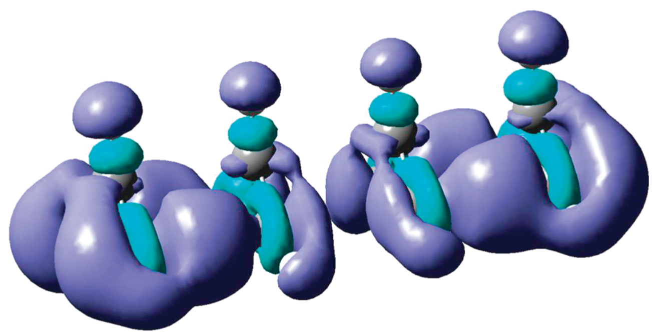

Figure 9. Electron density difference between the neutral and positive (+1) charged four C_3H_3 molecule array. The extensive and delocalized electron density suggests electron density disturbances is distributed across the array, suggesting the long-scale nature of excitations in the system.

Further investigation on the impact of c-direction elongation on DOS structure was also undertaken using the CASTEP module in the Materials Studio. Figure 8 shows the DOS plot of C_3H_3 units in a linear array along the c-direction. Each DOS plot is for a cell of $20 \times 20 \times c$, for c varying from 2.1 to 4.7 Å. From Figure 8, it is seen that the contour at the Fermi level changes greatly when c varies from 2.1 to 4.7 Å. When the distance between C_3H_3 units is larger than 2.9 Å along the c-direction, the DOS shows a more localized intense band above the Fermi level, reflecting isolated C_3H_3 character. When the distance between C_3H_3 units is in the range 2.5−2.9 Å along the c-direction, the DOS at the Fermi level increases significantly. This is consistent with the QM simulation, which has a minimum in the ground state energy of a C_3H_3 dimer at 2.7 Å separations. For a one-dimensional array of C_3H_3 units, when the interunit distance is 2.3 and 2.1 Å, Figure 8 shows the DOS intensity at the Fermi level is lower than that for an interunit distance of 2.5−2.9 Å. This suggests the tendency for forming bonds among C_3H_3 units. The delocalization of electron density across the array of C_3H_3 molecules is illustrated in Figure 9 where the electron density difference between the neutral and positive (+1) charged four C_3H_3 molecules is seen to be spread across the array.

In summary, both the QM simulations for a finite one-dimensional system and the periodic array of C_3H_3 units suggest that the excitation energy decreases inversely with the number of molecules in a linear array. Eventually, such excitation energies vanish as the number of molecules approaches infinity.

V. Conclusions

Generalized Dirac-like behavior in fermion systems was shown to follow from the scaling of low-lying, long spatial scale excitations in systems with degenerate ground states. While lattice structure affects the character of the ground states, it was shown that, even if interparticle forces are strong (and classic noninteracting quasi-particle concepts break down), scaling and degeneracy can evoke pseudorelativistic behaviors.

The generality of the approach indicates that such behaviors can exist in a variety of systems. Solids or thin films constituted of molecules with degenerate ground states[14−18] are likely candidates. Degeneracies that could also underlie these behaviors occur in arrays of interacting quantum dots,[41,42] and for bosons and fermions in optical lattices.[43] A re-examination of the present development suggests that pseudorelativistic behaviors could arise in boson systems. We suggest that a variety of pseudorelativistic quantum phenomena awaits exploration experimentally.

The results obtained in section II could also be applied to systems with nondegenerate ground states. In the presence of external applied fields, the expectation value of the single-particle momentum need not be zero.

Quantum computations on C_3H_3 showed that long-scale excitations have energy that decreases with characteristic length. If the single-particle momentum transition moments are independent of the long scale and the matrix elements of the correction to the potential (V_1) are small, then the excitation energy decreases inversely with the number of C_3H_3 in a linear way, as suggested in section IIIB. While the excitation energy does decrease with the number of molecules in the linear array, it does so in a more complex fashion. This is likely because of inaccuracies in the QM calculations for large numbers in the linear array and other factors (e.g., V_1, the structure of the transition moments, and possible higher order corrections from the scaling analysis, notably when the transition moments vanish).

Coarse-grained wave equations (section II) operate on long space−time scales. Thus a path integral method[12] based on the coarse-grained wave equation holds great promise for achieving long time simulations in many-particle quantum systems. Finally, the theory is not restricted to systems with degenerate ground states. The temporal response of a system subjected to a time-dependent, slowly varying external field could be examined to understand the long spatial scale migration of particles.

Acknowledgment. We appreciate the suggestions of Prof. K. Raghavachari regarding the QM computations and the choice of C_3H_3 as the demonstration system, as well as Profs. J. P. Allain, S. Kais, and J. Zaleski on systems with degenerate ground states. We appreciate the support of the Indiana University College of Arts and Sciences through general funding of the Center for Cell and Virus Theory. We appreciate the financial support from the Minority Leader Program from U.S. Air Force Research Lab, U.S. Department of Education Minority Science and Engineering Improvement Program.

References and Notes

(1) Ando, T. Theory of electronic states and transport in carbon nanotubes. *J. Phys. Soc. Jpn.* **2005**, *74* (3), 777–817.

(2) Ortoleva, P.; Iyengar, S. Multiscale theory of collective and single-particle modes in quantum nanosystem. *J. Chem. Phys.* **2008**, *128* (16), 164716.

(3) Pankavich, S.; Chen, Y.; Ortoleva, P. Multiscale theory of finite size bose systems: Implications for collective and single-particle excitations. *Phys. Rev. A* **2009**, *79* (1), 013628.

(4) Deutch, J. M.; Oppenheim, I. The concept of Brownian motion in modern statistical mechanics. *Faraday Discuss. Chem. Soc.* **1987**, *83*, 1–20.

(5) Shea, J. E.; Oppenheim, I. Fokker-Planck equation and non-linear hydrodynamic equations of a system of several Brownian particles in a non-equilibrium bath. *Physica A* **1997**, *247* (1−4), 417–443.

(6) Ortoleva, P. Nanoparticle Dynamics: A multiscale analysis of the Liouville equation. *J. Phys. Chem. B* **2005**, *109*, 21258–21266.

(7) Miao, Y.; Ortoleva, P. All-atom multiscaling and new ensembles for dynamical nanoparticles. *J. Chem. Phys.* **2006a**, *125*, 044901(8 pages).

(8) Miao, Y.; Ortoleva, P. Viral structural transitions: An all-atom multiscale theory. *J. Chem. Phys.* **2006b**, *125*, 214901.

(9) Pankavich, S.; Shreif, Z.; Ortoleva, P. Multiscaling for classical nanosystems: Definition of the Smoluchowski and Fokker-Planck equations. *Physica A* **2008**, (387), 4053–4069.

(10) Shreif, Z.; Ortoleva, P. P. Multiscale Derivation of an Augmented Smoluchowski Equation. *Physica A* **2009**, (388), 593–600.

(11) Pankavich, S.; Miao, Y.; Ortoleva, J.; Shreif, Z.; Ortoleva, P. Stochastic dynamics of bionanosystems: Multi-scale analysis and specialized ensembles. *J. Chem. Phys.* **2008**, *128*, 234908.

(12) Muller-Kirsten, H. *Introduction to Quantum Mechanics: Schrodinger Equation And Path Integral*; World Scientific Publishing Co.: Hackensack, NJ, 2006; ISBN: 951-256-691-0. Albeverio, S. A.; Hoegh-Krohn, R.; Mazzucchi, S. Mathematical Theory of Feynman Path Integrals: An Introduction; Lecture Notes in Mathematics; Springer: Germany, 2009; DOI: 10.1007/978-3-540-76956-9.

(13) Frisch, M. J. Trucks, G. W.; Schlegel, H. B.; Scuseria, G. E.; Robb, M. A. Cheeseman, J. R.; Montgomery, J. A., Jr.; Vreven, T.; Kudin, K. N.; Burant, J. C. Millam, J. M.; Iyengar, S. S.; Tomasi, J.; Barone, V.; Mennucci, B.; Cossi, M.; Scalmani, G.; Rega, N.; Petersson, G. A. Nakatsuji, H.; Hada, M.; Ehara, M.; Toyota, K.; Fukuda, R.; Hasegawa, J.; Ishida, M.; Nakajima, T.; Honda, Y.; Kitao, O. Nakai, H.; Klene, M.; Li, X.; Knox, J. E.; Hratchian, H. P.; Cross, J. B.; Bakken, V.; Adamo, C.; Jaramillo, J.; Gomperts, R.; Stratmann, R. E.; Yazyev, O.; Austin, A. J.; Cammi, R.; Pomelli, C.; Ochterski, J. W.; Ayala, P. Y. Morokuma, K.; Voth, G. A.; Salvador, P.; Dannenberg, J. J.; Zakrzewski, V. G.; Dapprich, S.; Daniels, A. D.; Strain, M. C.; Farkas, O.; Malick, D. K.; Rabuck, A. D.; Raghavachari, K.; Foresman, J. B.; Ortiz, J. V. Cui, Q.; Baboul, A. G.; Clifford, S.; Cioslowski, J.; Stefanov, B. B.; Liu, G.; Liashenko, A.; Piskorz, P.; Komaromi, I.; Martin, R. L.; Fox, D. J.; Keith, T. Al-Laham, M. A.; Peng, C. Y. Nanayakkara, A.; Challacombe, M.; Gill, P. M. W.; Johnson, B.; Chen, W.; Wong, M. W.; Gonzalez, C.; Pople, J. A. *Gaussian 03*, revision D.01; Gaussian, Inc.: Wallingford, CT, 2004.

(14) Seth, M.; Ziegler, T. Calculation of excitation energies of open-shell molecules with spatially degenerate ground states. II. Transformed reference via intermediate configuration Kohn-Sham time dependent density functional theory oscillator strengths and magnetic circular dichroism C terms. *J. Chem. Phys.* **2006**, *14* (124), 144105/1–144105/12.

(15) Kirtley, J. R.; Tsuei, C. C.; Ariando, H. J.; Smilde, H.; Hilgenkamp, H. Antiferromagnetic ordering in arrays of superconducting p-rings. *Phys. Rev. B: Condens. Matter Mater Phys.* **2005**, *21* (72), 214521/1–214521/11.

(16) Jiang, F.; Li, L.; George, T. F.; Sun, X. Effect of doping on carriers of conducting polymers with degenerate ground states. *Phys. Status Solidi B: Basic Res.* **2004**, *4* (241), 902–907.

(17) Matsuoka, H.; et al. Pseudo-octahedral high-spin Co(II) complexes with orbitally degenerate ground states as studied by SQUID and ESR spectroscopy. *Synth. Met.* **2003**, *1−3* (137), 1213–1214.

(18) An, Z.; Wu, Y. J.; Wu, C. Q. Charge-transfer in soliton and polaron states of phenyl-substituted polyacetylenes. *Synth. Met.* **2003**, *135−136*, 509–510.

(19) Jeffrey Hay, P.; Willard, R. Wadt Ab initio effective core potentials for molecular calculations. Potentials for K to Au including the outermost core orbitals. *J. Chem. Phys.* **1985**, *82*, 299.

(20) Axel, D. Becke Density-functional thermochemistry. III. The role of exact exchange. *J. Chem. Phys.* **1993)** , *98*, 5648.

(21) Hehre, W. J.; Ditchfield, R.; Pople, J. A. Self−Consistent Molecular Orbital Methods. XII. Further Extensions of Gaussian−Type Basis Sets for Use in Molecular Orbital Studies of Organic Molecules. *J. Chem. Phys.* **1972**, *56*, 2257.

(22) Krishnan, R.; Binkley, J. S.; Seeger, R.; Pople, J. A. Self-consistent molecular orbital methods. XX. A basis set for correlated wave functions. *J. Chem. Phys.* **1980**, *72*, 650.

(23) Woon, D. E.; Dunning, T. H., Jr. Gaussian basis sets for use in correlated molecular calculations. III. The atoms aluminum through argon. *J. Chem. Phys.* **1993**, *98*, 1358.

(24) Clark, T.; Chandrasekhar, J.; Spitznagel, G. W.; Schleyer, P. V. R. Efficient diffuse function-augmented basis sets for anion calculations. III. The 3-21+G basis set for first-row elements, Li-F. *J. Comput. Chem.* **2004**, *4* (3), 294.

(25) Frisch, M. J.; Pople, J. A. Self-consistent molecular orbital methods 25. Supplementary functions for Gaussian basis sets. *J. Chem. Phys.* **1984**, *80*, 3265.

(26) Bacon, A. D.; Zerner, M. C. An intermediate neglect of differential overlap theory for transition metal complexes: iron, cobalt and copper chlorides. *Theor. Chim. Acta* **1979**, *53* (1), 21–54.

(27) Stratmann, R. E.; Scuseria, G. E.; Frisch, M. J. An efficient implementation of time-dependent density-functional theory for the calculation of excitation energies of large molecules. *J. Chem. Phys.* **1998**, *109* (19), 8218–8224.

(28) Xu, B.; Yang, J.; Jiang, X.; Wang, Y.; Sun, H.; Yin, J. Ground and excited states calculations of 7-phenylamino-substituted coumarins. *J. Mol. Struct.* **2009**, *917* (1), 15–20.

(29) Martins, J. B. L.; Duraes, J. A.; Sales, M. J. A.; Vilela, A. F. A.; e Silva, G. M.; Gargano, Ricardo. Theoretical investigation of carotenoid ultraviolet spectra. *Int. J. Quantum Chem.* **2009**, *109* (4), 739–745.

(30) Ren, X.; Ren, A.; Feng, J.; Sun, C. A density functional theory study on photophysical properties of red light-emitting materials: Meso-substituted porphyrins. *J. Photochem. Photobiol., A: Chem.* **2009**, *203* (2−3), 92–99.

(31) Runge, E.; Gross, E. K. U. Density-functional theory for time-dependent systems. *Phys. Rev. Lett.* **1984**, *52* (12), 997–1000.

(32) Marques, M. A. L.; Gross, E. K. U. Time-dependent density functional theory. *Annu. Rev. Phys. Chem.* **2004**, *55*, 427–455.

(33) Casida, M. E. Time-dependent density functional response theory for molecules. *Recent Adv. Comput. Chem.* **1995**, *1* (Recent Advances in Density Functional Methods, Pt. 1), 155–192.

(34) Jacquemin, D.; Perpete, E. A.; Scuseria, G. E.; Ciofini, I.; Adamo, C. Extensive TD-DFT investigation of the first electronic transition in substituted azobenzenes. *Chem. Phys. Lett.* **2008**, *465* (4−6), 226–229.

(35) Wang, L. Y.; Chen, Q. W.; Zhai, G. H.; Wen, Z. Y.; Zhang, Z. X. Investigation of the structures and absorption spectra for some hemicyanine dyes with pyridine nucleus by TD-DFT/PCM approach. *THEOCHEM* **2006**, *778* (1−3), 15–20.

(36) Li, Y. L.; Han, L.; Mei, Y.; Zhang, J. Z. H. Time-dependent density functional theory study of absorption spectra of metallocenes. *Chem. Phys. Lett.* **2009**, *482* (4−6), 217–222.

(37) Karaca, S.; Elmaci, N. A theoretical study on the ground and excited state behaviors of TTBC related carbocyanine dyes. *THEOCHEM* **2009**, *915* (1−3), 149–159.

(38) Preat, J.; Jacquemin, D.; Wathelet, V.; Andre, J.-M.; Perpete, E. A. Towards the understanding of the chromatic behaviour of triphenylmethane derivatives. *Chem. Phys.* **2007**, *335* (2−3), 177–186.

(39) *Materials Studio 4.1, CASTEP Module*; Accelrys Inc.: San Diego, CA.

(40) Perdew, J. P.; Chevary, J. A.; Vosko, S. H.; Jackson, K. A.; Pederson, M. R.; Singh, D. J.; Fiolhais, C. Atoms, molecules, solids, and surfaces: Applications of the generalized gradient approximation for exchange and correlation. *Phys. Rev. B* **1992**, *46*, 6671–6687.

(41) Kuo, D. Tunneling current through multiple degenerate states of individual quantum dots. *Jpn. J Appl. Phys.* **2008**, *47*, 5358.

(42) Mikhailov, S. Two ground-state modifications of quantum-dot beryllium. *Theor. Phys. II*, **2002**, *66*, 153313−153316.

(43) Albus, A.; Illuminati, F.; Eisert, J. Mixtures of bosonic and fermionic atoms in optical lattices. *Phys. Rev. A: At., Mol. Opt. Phys.* **2003**, *2* (68), 023606/1–023606/11.

JP908441S